Geophysical Journal International

Geophys. J. Int. (2021) **225,** 1518–1529
Advance Access publication 2021 January 30
GJI General Geophysical Methods

doi: 10.1093/gji/ggab042

Detection and source parametrization of small-energy fireball events in Western Alps with ground-based infrasonic arrays

Giacomo Belli [1], Emanuele Pace [2,3] and Emanuele Marchetti [1]

[1] *Dipartimento di Scienze della Terra, Università degli Studi di Firenze, via G. La Pira,* 4, 50121 *Firenze, Italy. E-mail: g.belli@unifi.it*
[2] *Dipartimento di Fisica ed Astronomia, Università degli Studi di Firenze, via G. Sansone,* 1, 50019 *Sesto F.no, Firenze, Italy*
[3] *Osservatorio Polifunzionale del Chianti, Strada Provinciale Castellina in Chianti,* 50021 *Barberino val d'Elsa, Firenze, Italy*

Accepted 2021 January 28. Received 2021 January 27; in original form 2020 November 20

SUMMARY

We present infrasound signals generated by four fireball events occurred in Western Alps between 2016 and 2019 and that were recorded by small aperture arrays at source-to-receiver distances <300 km. Signals consist in a series of short-lived infrasonic arrivals that are closely spaced in time. Each arrival is identified as a cluster of detections with constant wave parameters (backazimuth and apparent velocity), that change however from cluster to cluster. These arrivals are likely generated by multiple infrasonic sources (fragmentations or hypersonic flow) along the entry trajectory. We developed a method, based on 2-D ray tracing and on the independent optically determined time of the event, to locate the source position of the multiple arrivals from a single infrasonic array data and to reconstruct the 3-D trajectory of a meteoroid in the Earth's atmosphere. The trajectories derived from infrasound array analysis are in excellent agreement with trajectories reconstructed from eyewitnesses reports for the four fireballs. Results suggest that the trajectory reconstruction is possible for meteoroid entries located up to ∼300 km from the array, with an accuracy that depends on the source-to-receiver distance and on the signal-to-noise level. We also estimate the energy of the four fireballs using three different empirical laws, based both on period and amplitude of recorded infrasonic signals, and discuss their applicability for the energy estimation of small energy fireball events (≤ 1kt TNT equivalent).

Key words: Infrasound; Numerical modelling; Wave propagation.

1 INTRODUCTION

Meteoroids of various sizes continuously enter the Earth's atmosphere with velocities ranging between 11 and 73.6 km s^{-1} (Drolshagen *et al.* 2020). Accurate detection of fireballs (or bolides, i.e. large bright meteors) is essential to accurately estimate the rate of meteoroid entries into the atmosphere and, therefore, also to assess the risk associated with the impact of large meteorites on the Earth surface.

Passing through the atmosphere, a meteoroid intensely vaporizes, due to thermal friction caused by interaction and impacts with the gas molecules and undergoes ablation (Ceplecha *et al*. 1998; Ceplecha & ReVelle 2005), mostly in the form of small solid fragments loss. Depending on its mass and velocity, the meteoroid may fragment in the last phases of its descent (Ceplecha *et al.* 1993; Brown *et al.* 1994; Borovička & Kalenda 2003), whenever the aerodynamic pressure exceeds the mechanical strength of the meteoroid (Bronshteyn 1995; Artemieva & Shuvalov 2001). These processes cause the bright light (meteor/fireballs) that is often reported at night.

Fireballs and meteors observations are traditionally carried out with optical techniques (Spurný *et al.* 2006; Cooke & Moser 2011), such as all-sky cameras. However such observations are possible only at night and in presence of favorable meteorological conditions.

Recently infrasonic detection of meteoroids and meteorites has gained attention (Brown *et al.* 2011; Silber *et al.* 2011; Le Pichon *et al.* 2013; Pilger *et al.* 2015; Pilger *et al.* 2020). Indeed, a meteoroid falling through the atmosphere produces infrasound, low frequency (< 20 Hz) sound, both during its hypersonic entry (Plooster 1970; Whitham 1974) and because of fragmentation episodes (Cumming 1989; Silber *et al.* 2018).

With an appropriate detection system, infrasound potentially allows us to identify meteoroids entries at any time of the day and under any weather conditions, making infrasound virtually able to ensure an almost continuous monitoring. Therefore, infrasound might contribute significantly to the estimate of the entry rate in the Earth's atmosphere not only of meteorites sized 1 m or more, on which previous and current research is mainly concerned (Silber *et al.* 2009; Pilger *et al.* 2020), but also of smaller meteoroids (<1 m), whose entry in the atmosphere is significantly more frequent (∼40 event per year at global scale for meteoroid diameter of 1 m, >100 events per year for meteoroids with a diameter of ∼0.5 m, Silber *et al.* 2009, Silber & Brown 2014).

Thanks to its high transmission efficiency in atmospheric waveguides (Drob *et al.* 2003), the infrasound generated by a meteoroid entry can be detected and recorded at very large distances from the source. For example, the Chelyabinsk meteorite (15 February 2013) released enough energy in the atmosphere, approximately 500 kt (Brown *et al.* 2013), to radiate low frequency infrasonic waves able to circle the globe twice and capable of being detected worldwide up to a distance of more than 85 000 km from the source (Le Pichon *et al.* 2013).

Infrasound can be used also to estimate the energy of the fireball events. As a matter of fact, several methods have been proposed to estimate the energy radiated by an explosive source on the basis of the infrasonic records (Whitaker 1995; ReVelle 1997; Edwards *et al.* 2006, Ens *et al.* 2012). They mostly consist of empirical laws derived from low altitude man-made nuclear or chemical explosions (Whitaker 1995; Blanc *et al.* 1997). By virtue of the impulsive and explosive nature of the meteoroid entry infrasound sources, these empirical relationships have been used also to estimate the amount of energy radiated by meteoroids in the atmosphere (Edwards *et al.* 2006; Le Pichon *et al.* 2013).

In this study, we present the analysis of infrasound signals generated by four fireball events observed in Northern Italy and investigate the potential of infrasound to detect and identify events, to reconstruct the meteoroid entry trajectory and, possibly, its energy. We chose events that were detected by the Italian all-sky camera network (PRISMA), or eyewitnessed and reported within the PRISMA bulletin (http://prisma.imo.net), and were also detected by infrasound arrays deployed in the Western Alps. We first present the infrasound network (Section 2) and the infrasound signature of selected events (Section 3). We propose a procedure to reconstruct the meteoroid trajectory from infrasound detected at a single array (Section 3). Eventually we estimate the energy of the four fireball events from recorded amplitudes and periods at maximum amplitude (Section 4), using three different empirical laws. We then compare the results and discuss the applicability of the energy estimation methods (Section 5).

2 INSTRUMENTAL SETUP AND DATA

The motion of a hypersonic object, with sizes greater than a few millimeters (Silber *et al.* 2018), into a fluid generates a hypersonic pressure front (the Mach cone), which creates an atmospheric shock wave (Le Pichon *et al.* 2002; Settles 2006). Additionally, collision with the air molecules causes the meteoroid to rapidly vaporize, leading to the formation of a cylindrical shock wave (Cumming 1989; Brown *et al.* 1996). Both shock waves turn into infrasound propagating away from the source (ReVelle 1976; Edwards *et al.* 2006; Edwards 2010).

In addition, at lower altitude, the meteoroid can fragment and radiate a blast wave (de Groot-Hedlin & Hedlin 2014), a shock wave with spherical, or quasi-spherical symmetry, typically generated by a point source (Needham 2010). Depending on its mass, composition, physical structure and velocity (Ceplecha *et al.* 1998), meteoroid terminal detonations typically occur at altitudes of 20–100 km. Larger meteorites penetrate deeper into the atmosphere, while smaller meteoroids typically fragment or burn out at higher altitudes (Halliday *et al.* 1989; Edwards *et al.* 2006; Gao & Mathews 2015).

The degree to which either mechanism, hypersonic flow or fragmentation, dominates infrasound production varies from event to event (Edwards *et al.* 2006; Silber & Brown 2014). For larger fireballs, the acoustic energy is mostly radiated in the region where the blast radius is larger, generally over a short section near the end of the luminous trajectory, where atmospheric penetration is deeper (Zinn *et al.* 2004; ReVelle 2005; Edwards *et al.* 2006), thus suggesting how fragmentation episodes dominate infrasound radiation. Nevertheless, Silber & Brown (2014) observed that hypersonic flow appears to dominate the infrasonic radiation of smaller meteoroids (grams to tens of kilograms).

It is often difficult to discriminate infrasound signals generated by meteoroids from the acoustic waves produced by other natural and anthropogenic sources. Therefore it is essential to improve the ability to distinguish the different infrasonic signatures and to discriminate signal from noise. This can be achieved by using an array of infrasonic sensors rather than a single microphone. For our study we used infrasonic data collected by three small-aperture (130–160 m) infrasonic arrays, deployed in the Western Alps (Fig. 1).

Two of these arrays (VLT and CHA) are located in Valle d'Aosta (Italy), near Valtournenche (45°52′50‘N, 7°38′15″E, 1850 m a.s.l.) and Champoluc (45°50′17‘N, 7°42′43″E, 2015 m a.s.l.) respectively (Figs 1d and b). Both arrays, operational since 2012, consist of four Optimic 2180 infrasonic fibre optic sensors, with a sensitivity of ∼100 mV Pa^{-1} and a flat frequency response between 1 Hz and 20 kHz. Infrasound data from the four sensors are collected with Guralp GMG-DM24 digitizer at 100 Hz.

The third infrasonic array is a five element, small aperture (161 m) array deployed in southern Switzerland's Canton Valais, nearby Leuk (46°17′49″N, 7°37′39″E, 750 m a.s.l., ILG, Fig. 1). The array was deployed in 2017 and it was working only in summer periods. ILG consists of a FIBRA infrasound array (www.item-geophysics.it), equipped with differential pressure transducers with a sensitivity of 400 mV Pa^{-1} in the pressure range of ±12.5 Pa and a flat frequency response between 0.01 and 200 Hz. Analogue pressure data are converted to digital, at each array element, at 50 Hz and 16 bits and are transmitted through fibre optic to a central unit, where data are recorded and GPS time stamped for time synchronization. To reduce the effect of wind noise all the arrays are deployed in forested areas and sensors had been installed into buried boxes.

In order to identify infrasonic events related to meteoroid entries, we extracted, from the set of infrasonic data recorded by the three arrays since their installation, all transient events that where consistent, both in term of timing and waveform characteristics, with fireball events optically observed and reported. In particular we used fireballs reports collected by PRISMA network (http://www.prisma.inaf.it/). PRISMA is an open project whose aim is to realize an Italian network of all-sky cameras for the observation and identification of fireballs. Bolide events reports collected by PRISMA are mainly based on images recorded by the all-sky cameras deployed throughout the Italian territory. However, PRISMA also collects the reports from amateur astronomers and citizens, through a dedicated website (http://prisma.imo.net), developed and maintened by Amrican Meteor Society (American Meteor Society - www.amsmeteors.org / International Meteor Organization - www.imo.net). On the basis of all collected eyewitness observational reports, PRISMA also reconstructs the meteoroid trajectory of each event as the average of all reports. Such a reconstruction is however strongly dependent on the number and quality of observations and is obviously affected by a significant uncertainty.

Out of the 66 fireballs, with at least 5 eyewitnesses reports, observed in Italy and reported on http://prisma.imo.net since 2016, we identified four infrasonic events with occurrence time and wave

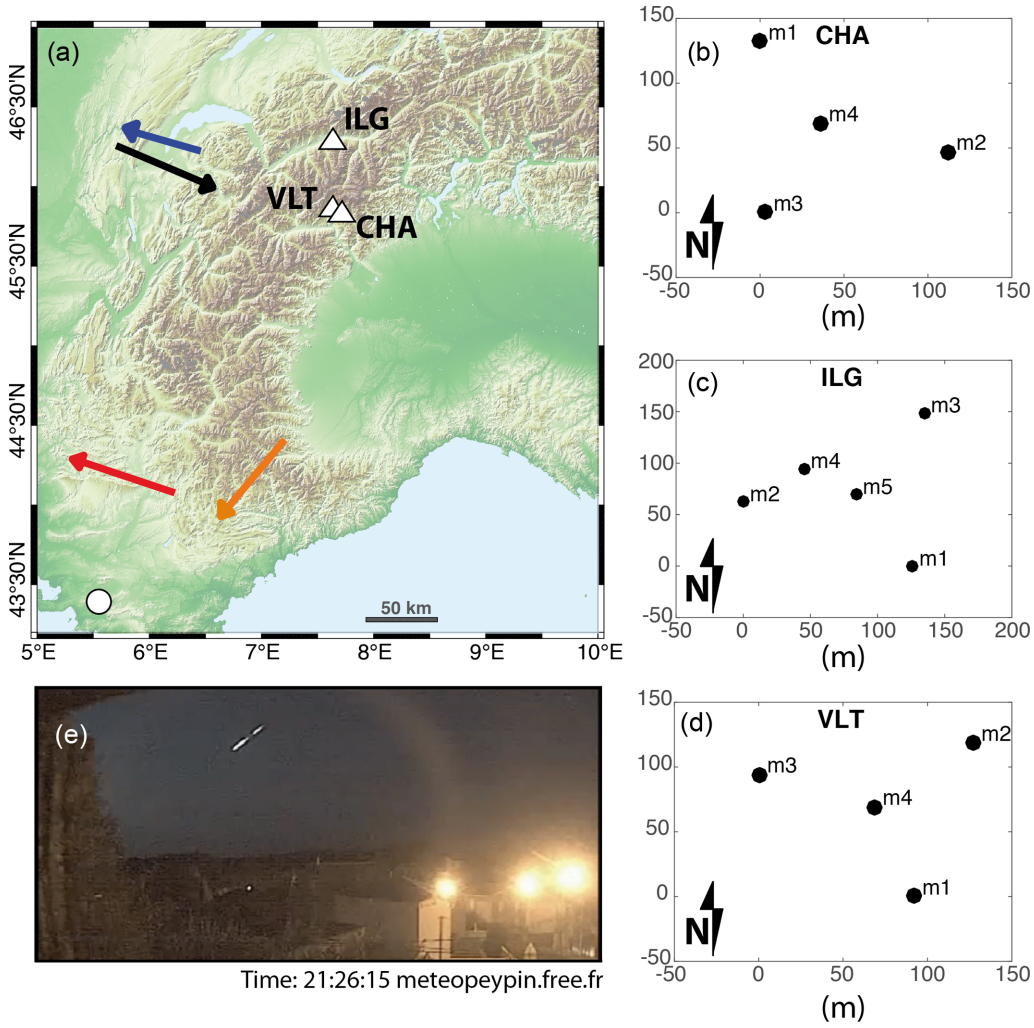

Figure 1. (a) A map of Western Alps showing the optical trajectories of the four analysed fireball events, reconstructed on http://prisma.imo.net, and the position of the three infrasonic arrays, VLT, CHA and ILG (white triangles). The bolides trajectories, reconstructed from eyewitness reports, are shown with arrows (orange for 2016/02/17, red for 2017/10/30, black for 2018/10/01 and blue for 2019/08/17). Panels (b), (c) and (d) show the geometry of CHA, ILG and VLT arrays; in these diagrams, values on the axis are in metres. (e) A photogram of the video (© Jean-Marie M.) of the 2019/08/17 fireball recorded in Peypin (France, with circle in a), giving the exact time of the event (19:26:14 UT).

Table 1. Onset time (t_o), optically determined and used for trajectory estimation and maximum peak-to-peak (pp) amplitudes and peak frequencies of the recorded infrasound signals of the four analysed bolide events.

Date	t_o (HH:MM:SS)	*pp* (Pa)	*f* (Hz)	v_w (m s^{-1})
2016/02/17	17:13:00	0.038	1.36	-1.5
2017/10/30	18:37:00	0.060	4.93	19.6
2018/10/01	22:37:00	2.90	1.04	7.7
2019/08/07	19:26:16	1.20	0.96	-3.8

characteristics consistent with those of a reported fireball event (Table 1, Figs 1 and 2).

3 METHODS: DATA ANALYSIS AND PROCESSING

3.1 Method: infrasound array data analysis

Array signal processing is based on the assumption that a signal is coherent at the different elements of an array, unlike noise, that does not show any correlation (Ulivieri *et al.* 2011). In our study, a multichannel correlation method was applied in the time domain to identify signals from noise and to characterize recorded signals in terms of wave parameters, backazimuth (B_{az}) and apparent velocity (c_a), of the infrasonic ray propagating across the array (Ulivieri *et al.* 2011; Marchetti *et al.* 2019).

We applied the procedure, discussed in detail in Ulivieri *et al.* (2011), on bandpass (1–10 Hz) filtered infrasound data recorded by the three arrays (CHA, VLT and ILG), considering successive 10 s time windows sliding with a superposition of 5 s. The 1–10 Hz bandpass filter was applied in order to optimize meteoroid signals detection above background noise. For each time window, the cross-correlation function, among the infrasound data recorded at the different array elements within the same time window, is calculated and the time residual for the corresponding lag time for sensor triplets is defined. For highly correlated signals the time residual tends to 0 and a detection of infrasound signal is defined.

Each detection is fully characterized in terms of degree of correlation, peak amplitude, backazimuth and apparent velocity

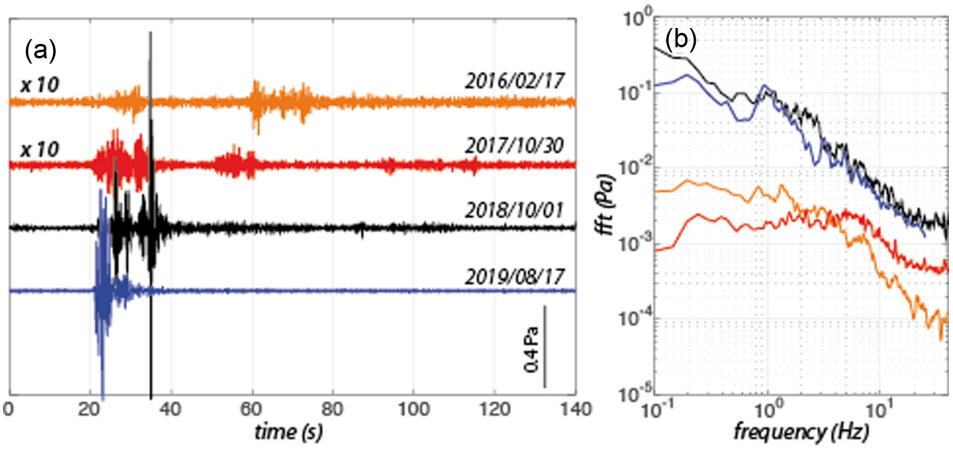

Figure 2. 1–10 Hz bandpass filtered waveforms (a) and corresponding spectra (b) computed with FFT (fast Fourier transform) of infrasound raw data recorded for the four analysed bolide events. In (a) waveform amplitudes of 2016 and 2017 bolides are multiplied by a factor 10 for better visualization.

(Fig. 3). The propagation backazimuth indicates the direction where the infrasonic ray comes from and points along the source-to-receiver direction. The apparent velocity is instead the velocity the infrasonic wave would have if it was propagating on the same plane of the array; it is related to real sound propagation speed (c) and to the take-off angle of the infrasonic ray (δ), measured in degrees from the vertical to the ground, according to:

$$c_a = \frac{c}{\sin\delta}, \tag{1}$$

According to eq. (1), the apparent velocity increases with decreasing the take-off angle, that results from the combination of source altitude and distance from the array.

The infrasound records of the four fireball events are shown in Fig. 3. Here, each event is recorded as separated clusters of detections (multiple detections closely spaced in times) that, considering the infrasound radiation of meteoroid entries, might represent multiple fragmentation processes or sections of the meteoroid trajectory where cylindrical shock wave is radiated. Obviously, array processing only provides the direction of infrasound propagation and not the position of the source. Therefore, the source location requires having detection from distinct arrays, in order to allow source location by cross-beam, or an independent observation of the event occurrence time.

3.2 Method: trajectory reconstruction from single array data

Considering the meteoroid typical hypersonic velocities of ∼20–60 km s^{-1} (Drolshagen *et al.* 2020), multiple sources of infrasound along the trajectory, produced by fragmentation episodes or meteor vaporization, might be tens of kilometers away from each other, even though very close in time (generally less than 1–2 s apart). Therefore, the observed delay (30–60 s) between subsequent infrasound detection clusters (arrivals) depends almost entirely on the different position of the infrasonic sources along the meteoroid trajectory, resulting in different source-to-receiver distances.

Similarly to what was proposed already by Silber & Brown (2014) and Pilger *et al.* (2020), we developed a method to reconstruct the trajectory of a meteoroid associated with multiple infrasonic arrivals, by using infrasonic data recorded by a single array. The basic assumptions are: (1) the entry trajectory of the meteoroid is a straight line; (2) radiation of infrasound by multiple sources along the meteoroid trajectory is synchronous and corresponds to the event occurrence time (t_0) provided by optical data; (3) delays between subsequent infrasound arrivals entirely depend on different propagation times from different sources to the same receiver; (4) each infrasound source is located along the ray path calculated with 2-D ray tracing modelling considering the real atmospheric specifications and the observed wave parameters; (5) a minimum of 2 arrivals are observed in the infrasound data.

In order to derive the position of the fragmentation events, once backazimuth and apparent velocity of the multiple arrivals are obtained, we apply a 2-D ray tracing, based on differential equations calculations that reconstruct the ray from subsequent spatial increments, considering the vertical profiles of sound speed and wind velocity at the time of the event.

Atmospheric specifications, from ground level to the thermosphere, are obtained combining numerical weather prediction (NPW) models for atmospheric pressure greater than 0.2 hPa, roughly corresponding to an altitude of 57 km, and empirical models of atmospheric physical features for the mesosphere and the thermosphere. For NWP we used ERA-Interim reanalysis data provided by the European Centre for Medium-Range Weather Forecasts (ECMWF). The model is based on 60 vertical levels from 1000 hPa down to 0.2 hPa, with a horizontal resolution of 0.75° and a temporal resolution of 6 hr (https://www.ecmwf.int). The model provides, among the others, air temperature (T), air density (ρ) as well as meridional and zonal winds at a given geo-potential pressure. For mesospheric and thermospheric models we used empirical temperatures and densities provided by NRLMSISE-00 model (Picone *et al.* 2002), while for the meridional and zonal wind components we used HWM-07 model (Drob *et al.* 2008). NWP and mesospheric and thermospheric models were combined following the procedure described by Schwaiger *et al.* (2019) to obtain the full atmospheric physical profile from ground to the thermosphere.

Atmospheric density (ρ) and pressure (p) are used to evaluate the adiabatic sound speed (c_T) at each given altitude (h), as defined by:

$$c_T(h) = \sqrt{\frac{\gamma p(h)}{\rho(h)}}, \tag{2}$$

where γ is the specific heat ratio of air, or adiabatic index, that we consider constant and equal to 1.4. The adiabatic sound speed

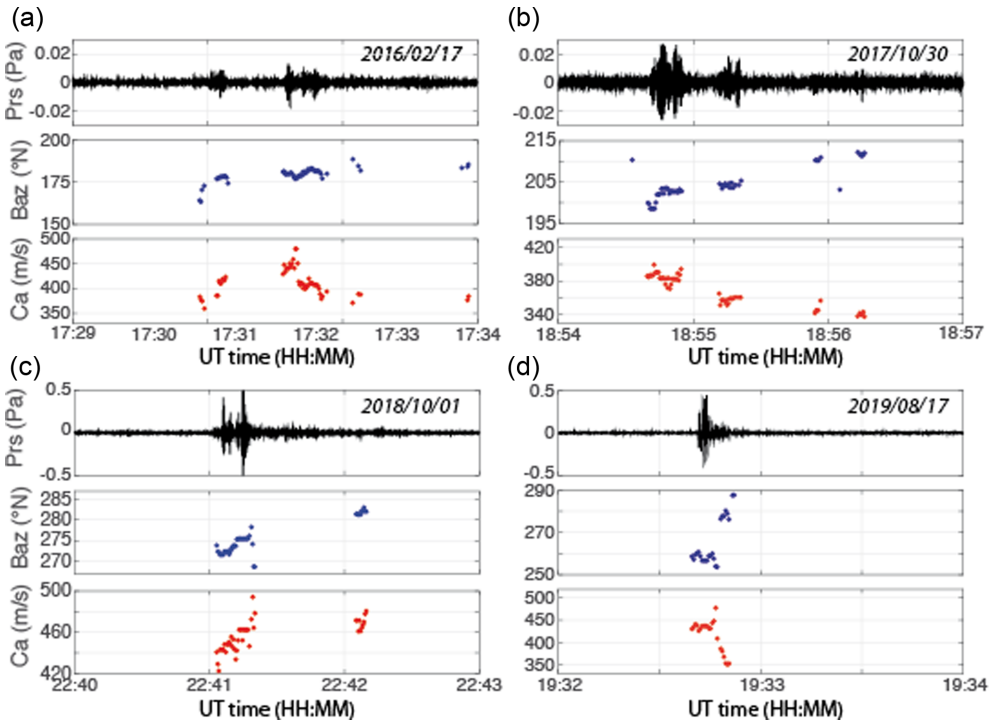

Figure 3. Infrasound record (black), bandpass filtered between 1 and 10 Hz, of the four fireballs events recorded at the arrays in Valle d'Aosta and in Switzerland. All events consist of 3–5 clusters of detections, that are identified with the array processing and characterized in terms of excess pressure at the array (black dots), backazimuth (blue dots) and apparent velocity (red dots) of infrasound detections. These clusters are typically 5–20 s long and are separated by delays of 5–60 s, thus resulting in a total signal duration <2–4 min. Each cluster of detections is characterized by almost constant backazimuth and apparent velocity values, that are however different from those of the adjacent clusters. Both backazimuth and apparent velocity values are arranged on a linear trend.

typically decreases with altitude in the troposphere, then increases in the stratosphere to reach a relative maximum in the stratopause and decreases again with altitude in the mesosphere, before finally increasing in the thermosphere. While an infrasonic wave is propagating in the atmosphere, the ray geometry is controlled by the sound velocity of the medium (Norris *et al.* 2010), as described by Snell's law. More precisely, refraction is governed by the effective sound speed (c_{eff}) (Fig. 4, Georges & Beasley 1977), that is defined as the adiabatic sound speed (c_T) summed to the wind component in the direction of wave propagation:

$$c_{\text{eff}} = c_T + (mw\cos\theta + zw\sin\theta), \tag{3}$$

where mw is meridional wind (oriented north–south and positive towards north), zw is the zonal wind (oriented west–east and positive towards east) and θ is the direction of infrasound wave propagation. A detailed discussion on infrasound propagation is beyond the scope of the present work and we thus refer to Drob *et al.* (2003) and references thereafter for specific reading.

For each meteoroid infrasound arrival, we calculate the source position by combing the reconstructed ray path with the traveltime that is simply calculated as the time difference between the arrival time and the optically determined fireball occurrence time (Fig. 4). Once location of at least two fragmentation episodes along two distinct rays is determined, the trajectory can be estimated through a 3-D linear interpolation. This is consistent with the assumption of a linear trajectory of the meteoroid.

3.3 Method: energy estimation

Infrasound waves can be used to estimate the energy released by a meteoroid entry. There are two main classes of empirical laws, that are based, respectively, on the period (ReVelle 1976, 1997; Ceplecha *et al.* 1998) or on the amplitude (Whitaker 1995; Clauter & Blandford 1998; Edwards *et al.* 2006; Ens *et al.* 2012) of recorded infrasound. One of the most used empirical period-energy relations was developed by the U.S. Air Force Technical Applications Center (AFTAC) and was subsequently adapted to fireballs (ReVelle 1997):

$$\log\left(\frac{E_s}{2}\right) = 3.34\log(P) - 2.58 \;\; \forall\; E_S \leq 200\; kt, \tag{4a}$$

$$\log\left(\frac{E_S}{2}\right) = 4.14\log(T) - 3.61 \;\forall\; E_S \geq 80\; kt, \tag{4b}$$

where E_S is the total source yield (in kilotons of equivalent TNT), expressing the total energy of the infrasonic wave source and T is the period (in seconds) of the recorded infrasound signal at its maximum amplitude. Such relation was derived for events with yield lower than 200 kt TNT (4a) or exceeding 80 kt TNT (4b).

In general, period based laws are to be considered more robust, especially in the case of a long range propagation, signal frequency being less affected than amplitude during atmospheric propagation (Mutschlecner *et al.* 1999). However, for less energetic fireball events ($E_S < 7$ kt TNT), amplitude-based laws are believed to be more appropriate, compared to period-based relationships (Edwards *et al.* 2006; Ens *et al.* 2012). Using a data set containing a wide variety of ground based chemical explosives yields as observed by the Los Alamos National Labs' infrasound network, Whitaker (1995) proposed an empirical relation between recorded infrasound and meteoroid yield:

$$\log E_S = 1.47\log\left(10^{kv_w}P\right) + \log(R) - 4.96, \tag{5}$$

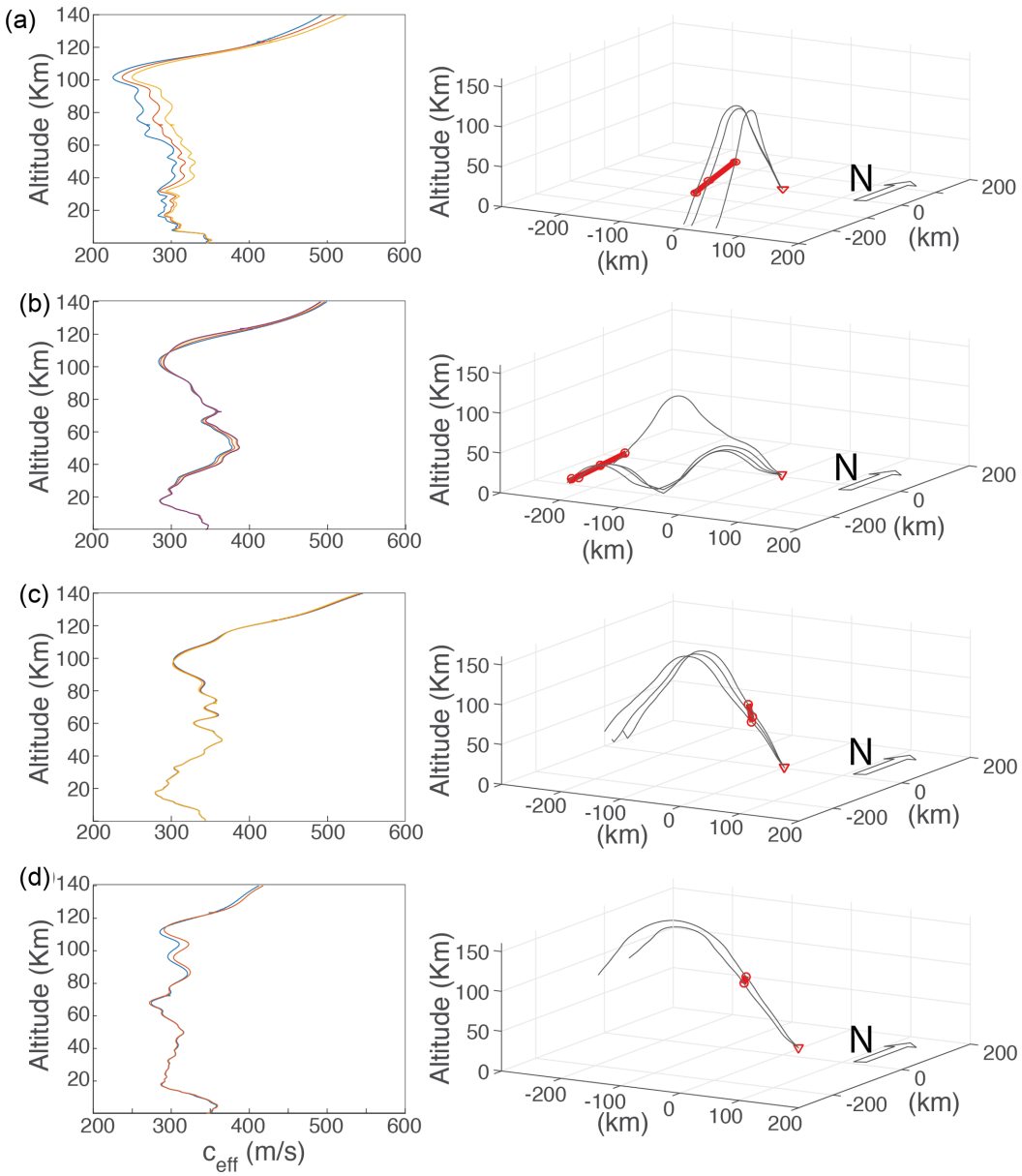

Figure 4. Vertical profiles of effective sound speed ($c_{\rm eff}$) in the atmosphere (left-hand panels) used to define the different infrasonic rays producing discrete arrivals identified within each infrasound signal (Table 2), then used to identify the position of the source of each infrasonic arrival. On the right-hand panel, we show ray paths obtained for the 2-D ray tracing (black lines), location of the infrasonic arrivals sources (red circles) and inferred 3-D trajectory of the fireball entry (red line). Location of the recording infrasound array is marked by a red triangle. Distances in the east/west and north/south directions are calculated from VLT array (Fig. 1).

where E_S is expressed in kt of equivalent TNT, P is the maximum peak-to-peak amplitude (in Pa) of the recorded infrasonic signal, $v_{\rm w}$ is the horizontal wind component along the ray path (m s^{-1}), k is an empirical constant for wind correction (in s m^{-1}, Mutschlecner & Whitaker 1990; Whitaker 1995; Edwards *et al.* 2006, Ens *et al.* 2012), while R is the source-to-receiver ground range in kilometres. For source energies $E_S \leq 7$ kt TNT, like the four fireball events analysed in this study, the given value of k is –0.0177 s m^{-1} (Edwards *et al.* 2006).

Similarly, from the analysis of a large number of fireballs detected simultaneously with both infrasonic arrays and satellite measurement, Edwards *et al.* (2006) derived:

$$E_S = 10^{3(a-kv_w)/b}\ R^3 P^{-3/b}, \tag{6}$$

where a and b are dimensionless empirical constants. In eq. (6), E_S is expressed in tons of TNT equivalent. For source energies $E_S \leq 7$ kt TNT, the values of k used also in eq. (5), a and b are –0.0177 s m^{-1}, 3.36 and –1.74, respectively (Edwards *et al.* 2006).

It is clear that amplitude-based eqs (5) and (6) strongly depend on propagation conditions, while eq. (4a), being based on the period of the recorded infrasound waveform is less dependent on propagation.

4 RESULTS

Recorded infrasound signals of the four identified fireballs are very different from event to event (Fig. 2). Events occurring closer to the array, such as the 2018 and 2019 fireballs, appear as large amplitude events (>1 Pa peak-to-peak) of short duration (<20 s)

and show transient features recalling blast waves (Needham 2010) (Fig. 2a). Events recorded at larger distance (>200 km), such as the 2016 and 2017 events, are characterized by smaller amplitudes (<0.05 Pa) and significantly longer durations (>60 s) and typically show multiple separated clusters of detections (Fig. 2a). Events also differ in the infrasound frequency content, with observed peak frequency spanning from 0.96 Hz, for the 2019 event, up to 4.93 Hz, for the 2017 events (Fig. 2b). Waveforms and wave parameters derived for the infrasound signals recorded for the four fireball events are presented in detail below.

4.1 Results: data processing

4.1.1 The 2016/02/17 fireball (17:18 UT)

Despite no all-sky camera images are available for this fireball, the event was widely observed by eyewitness in Western Alps. Based on the 122 reports of eyewitnesses in Italy, France and Switzerland, the meteoroid trajectory (∼NE–SW) and position, reconstructed on http://prisma.imo.net, are consistent with a theoretical backazimuth of ∼190–205°N (S–SE) and a distance of ∼200–250 km from the arrays (Fig. 1).

An infrasound signal compatible with this event is recorded starting 17:29 UT at VLT array. The ∼11 minutes time delay from the mean reporting time (17:18 UT) corresponds to a ∼200–250 km source-to-receiver distance.

Recorded infrasound consists in a sequence of three different arrivals recorded within 3 min (Fig. 3a). Each arrival is characterized by stable backazimuth and apparent velocity, that are however different among other arrivals. For this specific event, B_{az} increases with time from ∼175°N to ∼210°N. in good agreement with the optical trajectory (Fig. 1), with the meteoroid falling towards SW. Unlike backazimuth, apparent velocity, varying around 350–400 m s^{-1}, does not show any clear trend.

4.1.2 The 2017/10/30 fireball (18:39 UT)

Despite no all-sky camera images are available for this fireball, PRISMA collected 174 reports in Italy, France and Switzerland. The meteoroid trajectory (∼E–W) and position, reconstructed on http://prisma.imo.net, are consistent with a theoretical backazimuth of ∼205–220°N (SW) and a distance of ∼250 km from the array. The infrasonic signal generated by this meteoroid entry was recorded at VLT (Fig. 3b) array, from 18:54 UT. The ∼15 min time-shift from the mean reporting time (18:39 UT) corresponds to a source-to-receiver distance of ∼300 km.

Recorded infrasound consists of four, short-lasting (5–20 s) arrivals, recorded within ∼2 min. Arrival backazimuth is showing a systematic increase in time, from ∼197°N to ∼210°N, in good agreement with the east-west optical trajectory. Apparent velocity is showing a systematic decrease in time, from ∼390 to ∼340 m s^{-1}.

4.1.3 The 2018/10/01 fireball (22:30 UT)

Also for this event, no all-sky camera images are available. The trajectory (NW–E) and position, reconstructed on http://prisma.imo.net thanks to 16 available reports (Fig. 1), is consistent with a theoretical backazimuth of ∼290–280° N (W–NW) and a distance of ∼90–150 km from the CHA array (Figs 2a and 3c). The infrasound signal was recorded at CHA starting from about 22:40 UT (Fig. 3c). The ∼10 min time-shift from the mean reporting time (22:30 UT) agrees with a source-to-receiver distance of ∼200 km.

The recorded signal consists of three arrivals, with maximum amplitude of 0.5 Pa. The identified arrivals are marked by a clear variation of backazimuth, increasing with time, from 272°N to 284°N, in agreement with the NW–SE (∼280–290°N) reconstructed meteoroid trajectory (Fig. 1). Unlike for the previous events, apparent velocity is increasing almost continuously through time, from ∼440 to ∼470 m s^{-1}.

4.1.4 The 2019/08/17 fireball (19:26 UT)

For this event, recorded by ILG array, PRISMA collected 117 reports of eyewitness in Italy, France and Switzerland. The meteoroid trajectory (∼SE–NW) and position, reconstructed on http://prisma.imo.net (Fig. 1), are consistent with theoretical backazimuth of ∼265–275°N (West) and a distance of ∼90–140 km from the ILG array. Differently from the other three events, for this fireball event, a video of the bolide, recorded in Peypin (France) and uploaded on the American Meteor Society Website (© Jean-Marie M.), is available at https://prisma.imo.net/members/imo_view/event/2019/3842. This video provides the exact time of the event (t_0): 19:26:14 UT (Fig. 1e).

A clear signal was recorded at the ILG infrasound array at 19:32:42, with maximum amplitude of 0.4 Pa (Fig. 3d). The 388 s time delay from the exact event time (t_0) corresponds to a source-to-receiver distance of ∼120–130 km. The recorded signal consists of two arrivals with increasing (∼258°N–∼278°N) backazimuth and decreasing (∼440 m s^{-1}–∼370 m s^{-1}) apparent velocity. The observed backazimuth is in excellent agreement with the optical reconstruction of the trajectory.

4.2 Results: trajectory

Infrasound from the four analysed meteoroids (Table 1, Fig. 2) shows similar waveforms, that typically consist of multiple arrivals, characterized by distinct values of backazimuth and apparent velocity (Fig. 3). These features suggest that each arrival is likely generated by a single instantaneous source process (fragmentation or hypersonic flow) in a certain position along the trajectory. Different subsequent infrasound sources are required to explain the observed waveform.

Following the ray tracing based procedure presented in Section 3, we reconstruct the trajectory of the meteoroid source, by combining infrasound array wave parameters (t_i, B_{az} and c_a) of the different arrivals with onset time (t_o) provided by independent optical observations. Fig. 4 shows the reconstructed trajectories of the 4 meteoroids analysed in this work, showing the infrasound ray paths and the position of the source of each infrasonic arrival, identified once the infrasound source-to-receiver traveltime has been calculated.

The actual occurrence time (t_0) was available only for the 2019/08/17 fireball, while for the other events PRISMA provides only an average time obtained from multiple visual observation reports of numerous eyewitnesses. Therefore, for the trajectory reconstruction, we initially considered the optical onset time (t_0) reported on http://prisma.imo.net and progressively adjusted it to minimize residuals related to the best linear fit among the corresponding calculated positions of the sources of each infrasound arrival.

The trajectory reconstruction for the 2016/02/17 fireball was based on three different infrasonic rays (Table 2), corresponding

Table 2. Recording time (t_i), backazimuth (B_{az}), apparent velocity (c_a) and average horizontal wind velocity along source-to-receiver path (v_w) of the different infrasound arrivals of the recorded signals of the four bolides. The uncertainty on wave parameters values, resulting from the ∼150 m aperture of the three arrays, is ±1–2° for B_{az} and ±5–10 m s^{-1} for c_a. Position of the fragmentation source is expressed in terms of altitude (H), horizontal distance from the recording array (r) and travelled distance along the path (d). The sign of v_w indicates the direction of the wind with respect to the direction of propagation of the signal.

t_o	Infrasonic arrival	t_i (HH:MM:SS, UT)	B_{az} (°N)	c_a (m s^{-1})	H (km)	r (km)	d (km)
2016/2/17	#1	17:29:56	170	377	68	203	277
	#2	17:30:03	178	411	47	229	310
	#3	17:30:33	181	441	33	246	337
2017/10/30	#1	18:54:39	200	385	62	298	354
	#2	18:55:11	204	360	47	327	364
	#3	18:55:54	210	345	27	340	372
	#4	18:56:13	212	339	25	346	375
2018/10/1	#1	22:41:02	271	442	52	56	77
	#2	22:41:12	275	461	57	57	81
	#3	22:42:04	281	470	70	69	99
2019/8/17	#1	19:32:39	258	430	85	80	117
	#2	19:32:48	275	370	70	97	120

to three different arrivals (Fig. 3a). 2-D ray tracing predicts thermospheric refraction to the ground from an altitude of approximately 120 km (Fig. 4a). We obtain the best fit considering an onset time t_o = 17:13 UT. The trajectory, interpolated from the position of the three infrasonic episodes at altitudes between ∼75 and ∼35 km, is approximately NE–SW, forming an angle of ∼41° (α) to the North and an inclination angle (β) of ∼30° with the horizontal plan. The orientation (α, β) and position (∼200–250 km south from the VLT array) of the meteoroid trajectory (Fig. 5) are in excellent agreement with the optically trajectory estimated on the basis of eyewitness reports (Fig. 1).

For the 2017/10/30 fireball, we used the four different arrivals (Fig. 3b) to reconstuct four distinct rays. Based on B_{az} and c_a, 2-D ray tracing suggests that the ray corresponding to the highest altitude fragmentation episode reached the array after being refracted in the thermosphere at an altitude of ∼120 km, while the three rays obtained for lower c_a are refracted back to the ground from the stratosphere, at altitudes between ∼35 and ∼50 km (Fig. 4b). The best fit is obtained considering an onset time t_0 = 18:37 UT. Infrasound sources at altitude ranging from ∼66 and ∼24 km (Fig. 4b) are obtained, resulting into a meteoroid entrance approximately E-W (α ∼82°N) and with low inclination (β ∼25°). The trajectory reconstructed with infrasound (∼300–350 km from VLT, Fig. 5) is in excellent agreement with the optical trajectory estimated on the basis of eyewitness reports (Fig. 1).

The 2018/10/01 meteoroid trajectory reconstrutcion bases on three different reconstructed infrasonic rays (Table 2), corresponding to the three different recorded arrivals (Fig. 3c). The best fit is obtained considering an onset time t_0 = 22:37 UT and three infrasonic sources ranging from ∼75 and ∼50 km in altitude and with direct source-to-receiver infrasound propagation (Fig. 4c). The trajectory, obtained from 3-D linear fitting of the three obtained sources, is approaching the array approximately NW-SE (α ∼314°N), with an inclination angle of ∼46°. The trajectory orientation and position (Fig. 5) are in perfect agreement with the optical trajectory estimated on the basis of eyewitness reports (Fig. 1).

The 2019/08/17 meteoroid trajectory reconstruction was performed only with two infrasonic rays (Table 2), corresponding to the two arrivals (Fig. 3d). The exact onset time (t_o = 19:26:14 UT) is available for this fireball. The two sources are located at high elevation (87 and 70 km, respectively) with infrasound propagating to the array as direct waves (Fig. 4d). The reconstructed trajectory (α ∼146°N, β of ∼25°) and position (∼80–100 km from the ILG array, Fig. 5) are in perfect agreement with the optical reconstruction performed on the basis of eyewitness reports (Fig. 1).

4.3 Results: energy estimate

Meteoroids yields were estimated from infrasound records (Fig. 6) following the empirical relations described by eqs (4a), (5) and (6), based on period (ReVelle 1997) or on peak-to-peak amplitude (Whitaker 1995; Edwards *et al.* 2006) of recorded signal. We have chosen to use eq. (4a) rather than (4b) because it has been used successfully already by Pilger *et al.* (2020) for smaller meteorite yields, as low as 0.1 kt TNT. Period of the infrasound signal (Table 1) was obtained as the inverse of the frequency corresponding to the maximum amplitude of the FFT (fast Fourier transform) of raw infrasound data (Fig. 2b). In the amplitude related equations (eqs 5 and 6), we computed v_w as the average horizontal wind component along the source-to-receiver path, calculated between the altitude of the most energetic infrasound source and the ground (Table 1). For peak-to-peak amplitudes we used the values measured on fireballs infrasound raw data and reported in Table 1. Concerning the source-to-receiver distance, we used the horizontal distance (r in Table 2) for eq. (6) (Edwards *et al.* 2006), while we used the real propagation distance (d in Table 2) for eq. (5). In both cases, all distance values were derived from our reconstructed trajectories (Figs 4 and 5).

Inferred yield values (Fig. 6) span from a maximum of ∼6 tons down to ∼20 kg TNT Unfortunately, no independent yield estimates are available for the four identified fireball events. Therefore, data showed here can be used only for a qualitative comparison, that might however be useful to define a procedure for yield estimate of small size meteoroid entries.

5 DISCUSSION

Infrasonic array processing revealed that each infrasonic signal of the four analysed fireball events consists in a series of arrivals that we interpret being produced by different sources (fragmentation events

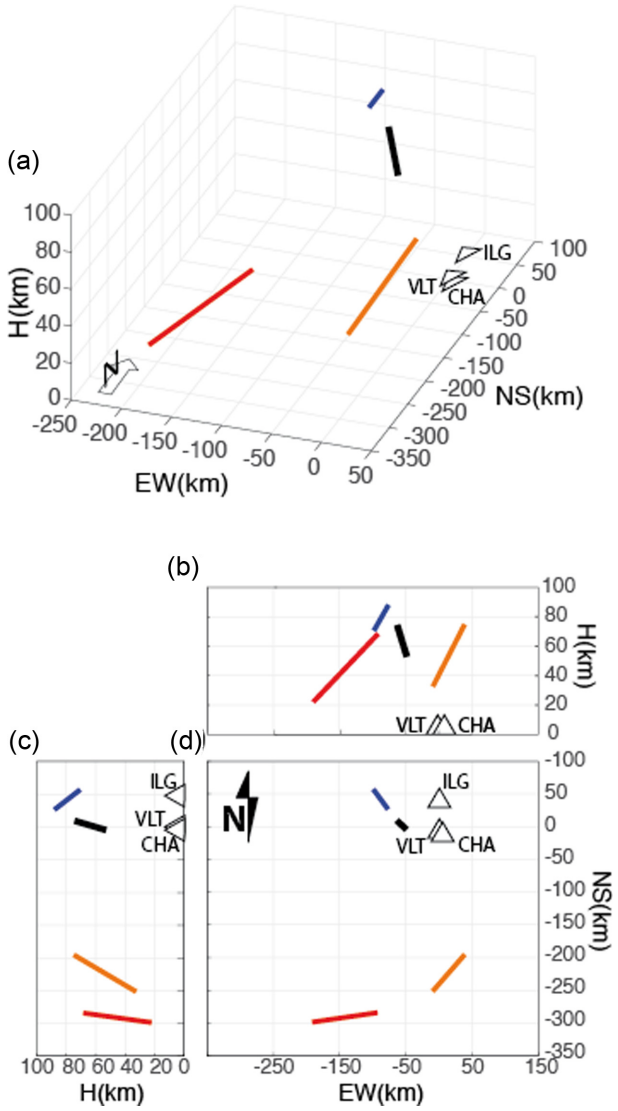

Figure 5. 3-D trajectory (a) of the four bolides (orange: 2016-02-17, red: 2017-10-30, black: 2018-10-01, blue: 2019-08-17) inferred from infrasound array observation. Position of the array is marked by the white triangles Projection of the 3-D trajectories on vertical sections oriented east/west (b) and north/south (c) and on the horizontal plane (d). The comparison of Fig. 5(d) with Fig. 1 highlights the general agreement between the infrasound-reconstructed trajectories and optical trajectories reconstructed on http://prisma.imo.net.

or hypersonic entry) along the entry trajectory and whose wavefield characteristics (B_{az}, c_a, t_i) are reflecting their mutual position.

Because of the hypersonic velocity, multiple infrasonic sources are nearly simultaneous Therefore, the first infrasonic arrival represents the signal that originated closest to the array, which might not necessarily coincide with the highest point along the meteor trajectory. This consideration allows us to correctly interpret the observed apparent velocity (Fig. 3), that is typically showing a variation trend. For the 2017/10/30 and the 2019/08/17 fireballs, the first arrival is associated with the largest incidence angle and apparent velocity is decreasing with time (Figs 3b and d) suggesting that the meteoroid lost altitude moving away from the array (VLT and ILG, respectively). In contrast, for the 2018/10/01 event we observe an increasing apparent velocity time trend (Fig. 3c), indicating that the closest infrasonic arrival source was likely located at lower altitude. This suggests that this meteoroid lost altitude approaching the array (CHA), in perfect agreement with eyewitness observations. For the 2016 event instead, the apparent velocity is not showing any clear trend, so that the direction of fall of this meteoroid is not as easily determined at first sight as it is for the other events.

A 2-D ray tracing approach, considering real atmospheric conditions, was used to define the position of the infrasonic sources of the different arrivals, identified at altitudes ranging between ∼90 and ∼25 km (Figs 5c and d). These values are in general agreement with theoretical predictions and empirical observation for small-to-medium size meteoroids (Halliday *et al.* 1989; Bland & Artemieva 2003; Edwards *et al.* 2006; Gao & Mathews 2015). The accuracy of infrasound source location presented here is related to the accuracy in evaluating wave parameters, to the accuracy of the propagation modelling and to the uncertainty of the predetermined t_0 of the event.

The recorded value of apparent velocity and backazimuth are indeed used to initiate the propagation modelling. In our case an accuracy of $\pm 3^\circ$ for the backazimuth and ± 10 m s^{-1} for the apparent velocity can be expected, resulting in an error of the location, of approximately 10 km. This could be reduced with larger aperture arrays, that do allow to estimate B_{az} and c_a more precisely.

Propagation modelling is controlled by the accuracy of input atmospheric features. For our work we used NWP and empirical models that are routinely used for infrasound propagation modelling. However Silber & Brown (2014) and Silber *et al.* (2015) showed that winds and small scale perturbations in the atmosphere affect infrasound propagation even in case of direct arrivals. Improvements might be obtained by applying full 3-D ray tracing and/or including small scale perturbances to the models. Such an effort is however beyond the scope of work, that aims to provide a simple and fast approach to estimate a meteoroid trajectory with a single array infrasonic data.

Fireball event t_0 is used to constrain the position of the infrasound source along the reconstructed ray path. t_0 is exactly known whenever all-sky cameras images or video of the fireball event are available, while the uncertainty on it can be very high (several minutes) in case of eyewitness reports. The largest misfit (7 min), between reported and modeled onset time, corresponds indeed to the 2018/10/01 fireball, for which only 16 reports were collected (http://prisma.imo.net).

Once the positions of the different infrasound sources have been calculated along the corresponding ray paths, the meteoroid trajectory can be obtained through 3-D linear interpolation. The accuracy of the trajectory reconstruction depends directly on the accuracy of the source location discussed above. Based on presented results, we suggest that the method is applicable for meteoroid-array maximum distances as large as ∼300 km. Indeed, with increasing distance the effect of the lateral variability of the atmospheric wind and temperature on the reconstruction accuracy gets progressively more impactive (Silber & Brown 2014). Moreover, for large distances, the multiple arrivals are recorded with very limited azimuth variation, reducing the efficiency of 3-D linear interpolation. Finally, the accuracy of the trajectory reconstruction depends on the aperture of the infrasonic array, as it is controlling the accuracy of the apparent velocity and backazimuth estimates.

Once an infrasound signal produced by a meteoroid entry has been identified and the meteoroid trajectory has been reconstructed, yield can be theoretically estimated from infrasound data. We applied three different methods, based both on the period (eq. 4, ReVelle. 1997) or on the amplitude (eq. 5, Whitaker 1995; eq. 6, Edwards *et al.* 2006) of infrasound data (Fig. 6).

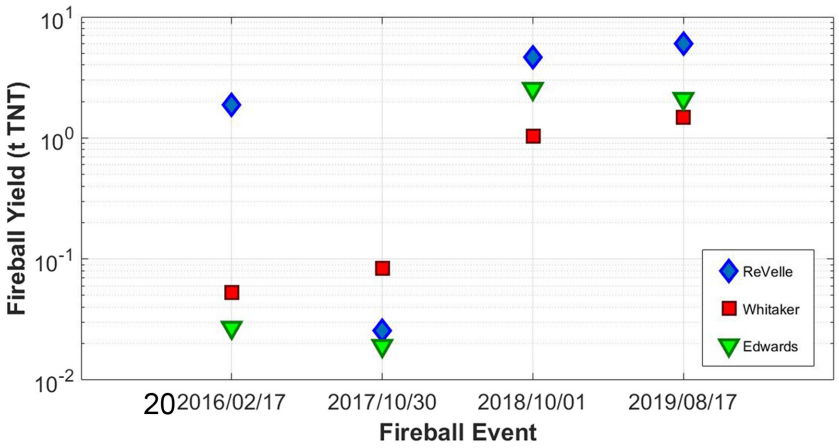

Figure 6. Yield (in ton of equivalent TNT) estimated for the four bolides based on the three methods commonly used (Whitaker 1995; ReVelle 1997; Edwards *et al.* 2006). The inferred yield values are spanning from ∼1–10 t TNT (10^{-3}–10^{-2} kt) for the 2018 and 2019 bolides, to 10–100 kg TNT (10^{-5}–10^{-4} kt TNT) for the 2016 and 2017 events.

Fig. 6 shows that the amplitude based methods (eqs 5 and 6) seem to produce almost comparable energy estimates for all analysed events. The period based method (eq. 4a) appears instead to yield significantly higher energy values for the 2016 event (1.9 t TNT compared to 25–50 kg TNT) and, to a lesser extent, also for the 2019 (6 t TNT compared to 1.5–2.1 t TNT) and for the 2018 (4.6 t TNT compared to 1–2.5 t TNT) fireballs.

This general overestimation, compared to the amplitude based methods (eqs 4 and 5), is probably due to the fact that the applicability of the period-based relationship is limited to large meteorites (ReVelle 1997), despite it has already been used successfully by Pilger *et al.* (2020) for small meteoroid yields (up to 0.1 kt TNT). Another reason of misfit might be related to wave propagation. Based on acoustically reconstructed trajectory (Fig. 4a), infrasound produced by the 2016 meteoroid entry likely underwent refraction at the thermosphere (Fig. 4a), where the high frequency component is preferentially absorbed (de Groot-Hedlin 2011). This is likely producing a passive enrichment of the lower frequencies, thus resulting in higher energy estimation.

Compared to the other methods, the amplitude based eq. (5) (Whitaker 1995) provides instead lower energy estimates for the 2016 and 2017 events. However, both events occurred far from the array (200–350 km) and generated infrasonic waves that underwent atmospheric refraction (Figs 4a and b). On the contrary, the 2018 and 2019 events, whose energy estimate computed with eq. (5) is in agreement with other approaches, occurred closer (≤100 km) to the array and produced direct infrasonic arrivals (Figs 4c and d). This likely results from the fact that eq. (5) (Whitaker 1995), being derived from ground-based explosion, is reasonably more appropriate for direct arrivals rather than stratospheric and thermospheric arrivals, for which a different infrasound attenuation should be considered. For the 2016 and 2017 fireballs events, more reliable results (∼50 and ∼80 kg TNT, respectively) are probably provided by eq. (6) (Edwards *et al.* 2006), derived from stratospheric ducted infrasound meteoroid signals.

However, since no independent energy estimate for the analysed fireball events is available, our results do not allow us to make absolute assertions on the robustness of the considered energy estimate methods. Nevertheless, we suggest that, for infrasound-based meteoroid yield estimates, any choice of the estimation method is absolutely premature if not preceded by an accurate reconstruction of the source-to-receiver infrasound propagation path.

For direct wave propagation we therefore suggest that eq. (5) (Whitaker 1995) is probably the most appropriate, while it likely loses accuracy with increasing source-to-receiver distance (>∼200 km), when applied to stratospheric or thermospheric arrivals. In the latter case, eq. (6) (Edwards *et al.* 2006), being derived from the analysis of stratospheric ducted infrasonic arrivals (Edwards *et al.* 2006), is reasonably more appropriate..

Eq. (4) (ReVelle 1997), which provides significantly higher energy estimates, compared to the other two empirical laws, for three out of the four fireball events analysed in this work, appears instead to be not very accurate and appropriate in case of meteoroid yields <10 t TNT. A more accurate period-based equation for small meteoroids energy estimation ($E_s \leq 10$ t TNT), derived from further analysis of several small meteoroid events, is thus probably to be determined.

6 CONCLUSION

We present an infrasound array analysis of four small fireball events recorded in Valle d'Aosta (Italy) and in Switzerland and reported on PRISMA fireballs website http://prisma.imo.net.

Array analysis showed that meteoroid entries are recorded as multiple arrivals, closely spaced in time and with variable backazimuth and apparent velocity. Based on the timing and wave parameters, we interpret them as the results of multiple infrasonic sources (fragmentation or hypersonic flow) along the entry trajectory.

We used 2-D ray tracing and real atmospheric specifications to model the meteoroid infrasound source positions, using data from a single array and the event onset time derived from independent optical or visual fireball observations. These source locations, at elevation ranging between ∼25 and ∼90 km and horizontal distances up to ∼300 km from the array, are eventually combined to derive the meteoroid entry trajectory with a 3-D linear fitting approach.

The reconstructed trajectories for the four analysed fireball events are in excellent agreement with the optical trajectory reconstructed by PRISMA on http://prisma.imo.net. Our trajectory reconstruction procedure, combining infrasound data and atmospheric physical features and structure, appears to be a very robust tool to approximately infer the actual trajectory of even smaller meteoroids through the Earth's atmosphere from infrasonic data of a single array. Obviously our method is strictly bound to the knowledge of the exact time of the event (t_0), and it is therefore applicable only in the case of

optically observed fireball events. This highlights clearly the need, but also the potential, of a synergistic research combining all-sky cameras and infrasonic array observations.

Eventually, we estimated the amount of energy radiated in the atmosphere by each of the four fireball events by using three different empirical laws based on infrasound (Whitaker 1995; ReVelle 1997; Edwards *et al.* 2006). The scattering observed (Fig. 6) and the lack of independent measurements of the event yield prevents us to discuss about the robustness of the different methods. Nevertheless, we suggest that, for infrasound-based meteoroid yield estimate, it is critical to locate the source and to reconstruct infrasound ray path as presented in Section 3. This is particularly critical for small events, where errors related to source location and propagation effect might strongly affect the yield estimate. For direct wave propagation, we suggest that Whitaker and Edwards procedures are likely providing reasonable results. ReVelle's method appears instead to be not very suitable for low energy ($\leq$ 10 t TNT) meteoroids yield estimation and a more appropriate period-based equation for small events energy estimation is thus probably necessary. For events recorded at larger source-to-receiver distances, and detected with infrasound signals that underwent refraction within atmospheric ducts, Whitaker's law is reasonably less appropriate and more data will be required to investigate its potential for infrasound-based yield estimate. Presented results highlight the lack of and the consequent need for a unique and more appropriate law for small fireball energy estimates. We suggest that this must be achieved from the analysis of several events detected simultaneously with all-sky cameras and infrasound arrays, previously organized in distinct event classes, appropriately separated by virtue of the corresponding infrasound propagation mode, reconstructed by means of an accurate ray tracing.

ACKNOWLEDGEMENTS

We thank Rotary San Casciano Chianti (http://www.rotarysancascianochianti.org/) and Fondazione Cassa di Risparmio di Firenze for having supported and allowed the realization of this research activity by providing a scholarship. PRISMA network (http://www.prisma.inaf.it/) and American Meteor Society (https://www.amsmeteors.org/) are greatly acknowledged for providing the fireball events optical eyewitnesses data set. We are grateful to Maurizio Ripepe and Daniele Gardiol for the valuable advices they gave to our research, as well as to Christoph Pilger and Elizabeth Silber for their helpful comments to an early version of the manuscript. This study was facilitated by previous research performed within the framework of the ARISE project (Blanc *et al.* 2018), funded by the European Commission within the FP7 and Horizon 2020 programs (Grant agreements 284387 and 653980). Infrasound data, recorded by VLT, CHA and ILG arrays, used to achieve all the findings and create all the figures in this paper, are freely available in the Open Science Framework repository (https://osf.io/fqtk7/).

REFERENCES

Artemieva, N. A. & Shuvalov, V. V., 2001. Motion of a fragmented meteoroid through the planetary atmosphere, *J. geophys. Res.,* **106**(E2), 3297–3309.

Blanc, E., Perez, S., Issartel, J. P. & Millies-Lacroix, J. C., 1997. Detection of nuclear explosions in the atmosphere, *Chocs,* 23–34.

Blanc, E. *et al.* 2018. Toward an improved representation of middle atmospheric dynamics thanks to the ARISE project, *Surv. Geophys.,* **39,** 171–225.

Bland, P. A. & Artemieva, N. A., 2003. Efficient disruption of small asteroids by Earth's atmosphere *Nature,* **424,** 288–291, doi:10.1038/nature01757, 0028-0836.

Borovicĥka, J. & Kalenda, P., 2003. The Morávka meteorite fall: 4. Meteoroid dynamics and fragmentation in the atmosphere, *Meteor. Planet. Sci.,* **38**(7), 1023–1043.

Bronshteyn, V. A., 1995. Fragmentation and crushing of large meteoric bodies in an atmosphere, *Solar Syst. Res.,* **29,** 392–399.

Brown, P., Ceplecha, Z., Hawkes, R. L., Wetherill, G., Beech, M. & Mossman, K., 1994. The orbit and atmospheric trajectory of the Peekskill meteorite from video records, *Nature,* **367**(6464), 624.

Brown, P. *et al.*, 1996. The fall of the St-Robert meteorite, *Meteor. Planet. Sci.,* **31**(4), 502–517.

Brown, P. *et al.* 2011. The fall of the Grimsby meteorite—I: fireball dynamics and orbit from radar, video, and infrasound records, *Meteor. Planet. Sci.,* **46**(3), 339–363.

Brown, P. G. *et al.* 2013. A 500-kiloton airburst over Chelyabinsk and an enhanced hazard from small impactors, *Nature,* **503**(7475), 238–241.

Ceplecha, Z., Borovička, J., Elford, W. G., ReVelle, D. O., Hawkes, R. L., Porubčan, V. & Šimek, M., 1998. Meteor phenomena and bodies, *Space Sci. Rev.,* **84**(3-4), 327–471.

Ceplecha, Z. & ReVelle, D. O., 2005. Fragmentation model of meteoroid motion, mass loss, and radiation in the atmosphere, *Meteor. Planet. Sci.,* **40**(1), 35–54.

Ceplecha, Z., Spurny, P., Borovicka, J. & Keclikova, J., 1993. Atmospheric fragmentation of meteoriods, *Astron. Astrophys.,* **279,** 615–626.

Clauter, D. & Blandford, R., 1998. Capability modeling of the proposed international system 60-station infrasonic network, in *Proceedings of the Infrasound Workshop for CTBT Monitoring,* Los Alamos National Laboratory report LA-UR-98-56.

Cooke, W. J. & Moser, D. E., 2011, The status of the NASA all sky fireball network, in *Proceedings of the International Meteor Conference,* Sibiu, Romania, 15–18 September 2011, eds Gyssens, M. & Roggemans, P. International Meteor Organization, ISBN 2978-2-87355-023-3, pp. 9–12.

Cumming, G. L., 1989. Alberta bolide of June 1, 1982: interpretation of photographic and seismic records, *Can. J. Earth Sci.,* **26**(7), 1350–1355.

de Groot-Hedlin, C., Hedlin, M. A. & Walker, K., 2011. Finite difference synthesis of infrasound propagation through a windy, viscous atmosphere: application to a bolide explosion detected by seismic networks, *Geophysical Journal International,* **185,** 305–320.

de Groot-Hedlin, C. D. & Hedlin, M. A., 2014. Infrasound detection of the Chelyabinsk meteor at the USArray, *Earth Planet. Sci. Lett.,* **402,** 337–345.

Drob, D. P., Picone, J. M. & Garces, M., 2003. Global morphology of infrasound propagation, *J. geophys. Res.,* **108**(21), doi:10.1029/2002JD003307.

Drob, D. P. *et al.*, 2008. An empirical model of the Earth's horizontal wind fields: HWM07, *J. geophys. Res.,* **113**(A12),.

Drolshagen, E., Ott, T., Koschny, D., Drolshagen, G., Schmidt, A. K. & Poppe, B., 2020. Velocity distribution of larger meteoroids and small asteroids impacting Earth, *Planet. Space Sci.,* **184,** 104869, doi:10.1016/j.pss.2020.104869.

Edwards, W. N., 2010. Meteor generated infrasound: theory and observation, in *Infrasound Monitoring for Atmospheric Studies,* pp. 361–414. Springer.

Edwards, W. N., Brown, P. G. & ReVelle, D. O., 2006. Estimates of meteoroid kinetic energies from observations of infrasonic airwaves, *J. Atmos. Solar-Terrest. Phys.,* **68**(10), 1136–1160.

Ens, T. A., Brown, P. G., Edwards, W. N. & Silber, E. A., 2012. Infrasound production by bolides: a global statistical study, *J. Atmos. Solar-Terrest. Phys.,* **80,** 208–229.

Gao, B. & Mathews, J. D., 2015. High-altitude meteors and meteoroid fragmentation observed at the Jicamarca Radio Observatory, *Mon. Not. R. Astron. Soc.,* **446**(4), 3404–3415.

Georges, T. M. & Beasley, W. H., 1977. Refraction of infrasound by upper-atmospheric winds, *J. acoust. Soc. Am.,* **61**(1), 28–34.

Halliday, I., Blackwell, A. T. & Griffin, A. A., 1989. The typical meteorite event, based on photographic records of 44 fireballs, *Meteoritics,* **24**(2), 65–72.

Le Pichon, A., Ceranna, L., Pilger, C., Mialle, P., Brown, D., Herry, P. & Brachet, N., 2013. The 2013 Russian fireball largest ever detected by CTBTO infrasound sensors, *Geophys. Res. Lett.,* **40**(14), 3732–3737.

Le Pichon, A., Garcés, M., Blanc, E., Barthélémy, M. & Drob, D. P., 2002. Acoustic propagation and atmosphere characteristics derived from infrasonic waves generated by the Concorde, *J. acoust. Soc. Am.,* **111**(1), 629–641.

Marchetti, E. *et al.* 2019. Infrasound array analysis of debris flow activity and implication for early warning, *J. geophys. Res.,* **124**(2), 567–587.

Mutschlecner, J. P. & Whitaker, R. W., 1990, The correction of infrasound signals for upper atmospheric winds, No. LA-UR-90-1997; CONF-9005236–2, Los Alamos National Lab., NM, USA.

Mutschlecner, J. P., Whitaker, R. W. & Auer, L. H., 1999, An empirical study of infrasonic propagation, No. LA-13620-MS, Los Alamos National Lab., Los Alamos, NM, USA.

Needham, C. E., 2010. *Blast Waves,* Vol. **402,** Springer.

Norris, D., Gibson, R. & Bongiovanni, K., 2010. Numerical methods to model infrasonic propagation through realistic specifications of the atmosphere, in *Infrasound Monitoring for Atmospheric Studies,* pp. 541–573. Springer.

Picone, J.M., Hedlin, A.E., Drob, D.P. & Aikin, A.C., 2002, NRLMSISE-00 empirical model of the atmosphere: statistical comparison and scientific issues, *J. geophys. Res.,* **107,** A12, doi:10.1029/2002JA009430.

Pilger, C., Ceranna, L., Ross, J. O., Le Pichon, A., Mialle, P. & Garcés, M. A., 2015. CTBT infrasound network performance to detect the 2013 Russian fireball event, *Geophys. Res. Lett.,* **42**(7), 2523–2531.

Pilger, C., Gaebler, P., Hupe, P., Ott, T. & Drolshagen, E., 2020. Global monitoring and characterization of infrasound signatures by large fireballs, *Atmosphere,* **11**(1), 83.

Plooster, M. N., 1970. Shock waves from line sources. Numerical solutions and experimental measurements, *Phys. Fluids,* **13**(11), 2665–2675.

ReVelle, D. O., 1976. On meteor-generated infrasound, *J. geophys. Res.,* **81**(7), 1217–1230.

ReVelle, D. O., 1997, Historical detection of atmospheric impacts by large bolides using acoustic-gravity waves, No. LA-UR-95-1263; CONF-9504147-1, Los Alamos National Lab., NM, USA.

ReVelle, D. O., 2005. Recent advances in bolide entry modeling: a bolide potpourri, in *Modern Meteor Science An Interdisciplinary View,* pp. 441–476. Springer.

Schwaiger, H.F., Iezzi, A.M. & Fee, D, 2019, AVO-G2S: a modified, open-source ground-to-space atmospheric specification for infrasound modeling, *Comput. Geosci.,* **125,** 90–97.

Settles, G. S., 2006. High-speed imaging of shock waves, explosions and gunshots: new digital video technology, combined with some classic imaging techniques, reveals shock waves as never before, *Am. Sci.,* **94**(1), 22–31.

Silber, E. A., Boslough, M., Hocking, W. K., Gritsevich, M. & Whitaker, R. W., 2018. Physics of meteor generated shock waves in the Earth's atmosphere—a review, *Adv. Space Res.,* **62** (3), 489–532.

Silber, E. A. & Brown, P. G., 2014. Optical observations of meteors generating infrasound—I: acoustic signal identification and phenomenology, *J. Atmos. Solar-Terrest. Phys.,* **119,** 116–128.

Silber, E. A., Brown, P. G. & Krzeminski, Z., 2015. Optical observations of meteors generating infrasound: weak shock theory and validation, *J. geophys. Res.,* **120**(3), 413–428.

Silber, E. A., Le Pichon, A. & Brown, P. G., 2011. Infrasonic detection of a near-Earth object impact over Indonesia on 8 October 2009, *Geophys. Res. Lett.,* **38**(12),.

Silber, E. A., ReVelle, D. O., Brown, P. G. & Edwards, W. N., 2009. An estimate of the terrestrial influx of large meteoroids from infrasonic measurements, *J. geophys. Res.,* **114**(E8), doi:10.1029/2009JE003334.

Spurný, P., Borovička, J. & Shrbený, L., 2006. Automation of the Czech part of the European fireball network: equipment, methods and first results, *Proc. Int. Astron. Un.,* **2**(S236), 121–130.

Ulivieri, G., Marchetti, E., Ripepe, M., Chiambretti, I., De Rosa, G. & Segor, V., 2011. Monitoring snow avalanches in Northwestern Italian Alps using an infrasound array, *Cold Regions Sci. Technol.,* **69**(2-3), 177–183.

Whitaker, R. W., 1995. *Infrasonic monitoring,* No. LA-UR-95-2775, Los Alamos National Lab., NM, USA.

Whitham, G. B., 1974, *Linear and Nonlinear Waves,* John Wiley & Sons. Inc.

Zinn, J., O'Dean, P. J. & ReVelle, D. O., 2004. Leonid meteor ablation, energy exchange, and trail morphology, *Adv. Space Res.,* **33**(9), 1466–1474.